

2. Dynamo models

Chris Jones
Department of Applied Mathematics

University of Leeds, UK

Nordita Winter School January 12th Stockholm

Dynamo simulations

Solve induction equation and the Navier-Stokes equations simultaneously. Most work has been done on convection-driven dynamos.

Anti-dynamo theorems tell us dynamo process is three-dimensional, so expect 3D magnetic fields.

(i) No dynamo can be maintained by a planar flow

$$(u_x(x, y, z, t), u_y(x, y, z, t), 0).$$

No restriction is placed on whether the field is 2D or not in this theorem.

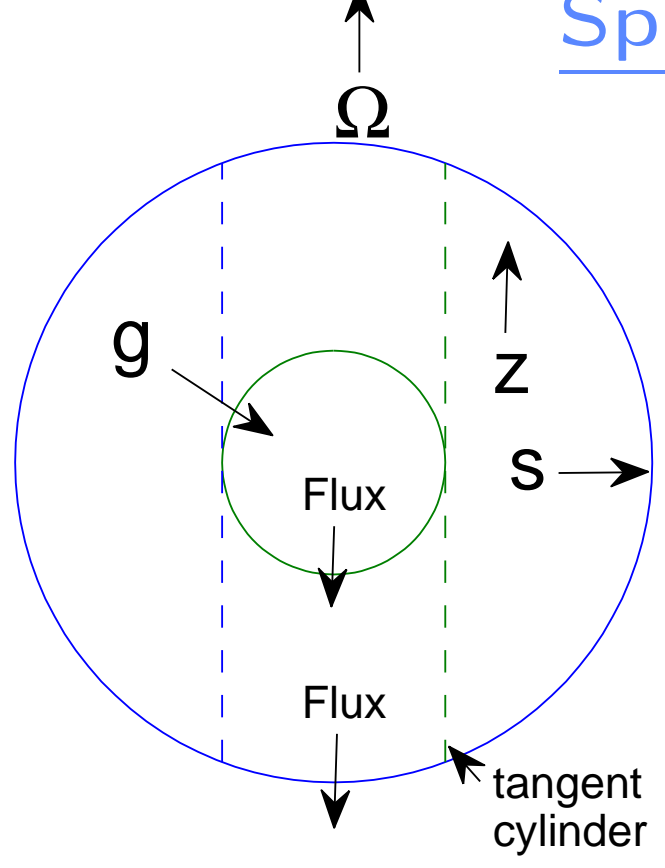
- (ii) Cowling's theorem. An axisymmetric magnetic field vanishing at infinity cannot be maintained by dynamo action.
- (iii) A purely toroidal flow, that is one with $\mathbf{u} = \nabla \times T\mathbf{r}$ cannot maintain a dynamo. Note that this means that there is no radial motion, $u_r = 0$.

In the Earth's core, the flow is clearly 3D, and rotating convection leads to 3D flows.

Simulations are therefore computationally demanding, and require clusters of processors for serious study. Only models close to critical can be studied with desktop machines.

Parallel programming (MPI) is required, and code construction is challenging.

Spherical geometry



Rotating about z-axis. Gravity radially inward, $g=g_0r$. Centrifugal acceleration small. Length scale d is gap-width from inner to outer boundary. Convection usually onsets outside tangent cylinder.

Radius ratio inner/outer core for Earth is 0.35. Codes formulated in spherical polars r, θ , ϕ , but cylindrical coordinates s, ϕ , z also useful.

Inner core boundary at r = 7/13 = 0.538, CMB at r = 20/13 = 1.538.

Dimensionless equations of the model

We use the magnetic diffusion time d^2/η as the unit if time. The unit of velocity is then η/d , so the dimensionless velocity is a direct measure of the magnetic Reynolds number. The unit of magnetic field is $(\Omega \rho \mu_0 \eta)^{1/2}$ so a magnetic field of strength 1 has an Elsasser number of 1. Recall that in the Earth's core this unit is about 14 Gauss.

The dimensional Boussinesq equation of motion is

$$\rho \frac{D\mathbf{u}}{Dt} + 2\rho\Omega \times \mathbf{u} = -\nabla p + \mathbf{j} \times \mathbf{B} + \rho\nu\nabla^2\mathbf{u} + \rho g(\alpha T + \xi)\hat{\mathbf{r}}.$$

The buoyancy term has a thermal part αT , α being the coefficient of thermal expansion, and a compositional component ξ , where ξ is the mass fraction of light material (believed to be sulphur and oxygen in the core)

Model equations 4/36

The dimensionless form is

$$\frac{E}{Pm}\frac{D\mathbf{u}}{Dt} + 2\hat{\mathbf{z}} \times \mathbf{u} = -\nabla p + (\nabla \times \mathbf{B}) \times \mathbf{B} + E\nabla^2\mathbf{u} + \frac{RaPm}{Pr}(T + \xi)\mathbf{r}$$

Here the unit of temperature is ΔT , the superadiabatic temperature difference across the core, and the unit of ξ is $\alpha \Delta T$.

Ekman number $E=\nu/\Omega d^2~\sim 3\times 10^{-9}~(10^{-15})$

Modified Rayleigh number $Ra = \frac{g\alpha\Delta T'd}{\Omega\kappa} \sim 10^3~(10^9)$

Prandtl number $Pr = \nu/\kappa \quad \sim 1$

Magnetic Prandtl number $Pm = \nu/\eta \sim 1 \ (2 \times 10^{-6})$

 η magnetic diffusivity, u turbulent kinematic viscosity,

 κ is the turbulent thermal diffusivity.

Model equations 5/36

Estimate for the Rayleigh number comes from

$$Ra = PrPm^{-1}g\alpha\Delta Td/\Omega\eta \sim 10 \times 10^{-5} \times 10^{-3} \times 2 \times 10^{6}/7 \times 10^{-5} \times 2$$

$$\sim PrPm^{-1} \times 10^3$$

Note that ΔT is not the actual temperature difference across the core, but only the temperature difference above the adiabatic part which is very much smaller.

Induction equation

$$\frac{\partial \mathbf{B}}{\partial t} = \nabla^2 \mathbf{B} + \nabla \times (\mathbf{u} \times \mathbf{B})$$

Temperature and composition equations

$$\frac{\partial T}{\partial t} = \frac{Pm}{Pr} \nabla^2 T - \mathbf{u} \cdot \nabla T + Q, \quad \frac{\partial \xi}{\partial t} = \frac{Pm}{Pc} \nabla^2 \xi - \mathbf{u} \cdot \nabla \xi + Q_{\xi}$$

Continuity equations

$$\nabla \cdot \mathbf{B} = \nabla \cdot \mathbf{u} = 0$$

Here $Pc = \nu/\kappa_{\xi}$, κ_{ξ} being the compositional diffusion: Pc is large.

Model equations 6/36

If we assume turbulent values of diffusivities, with Prandtl numbers unity, T and ξ can be added to form co-density variable. Note this assumes boundary conditions are the same.

Q and Q_{ξ} are internal heating sources and composition sources, if any.

Simplest assumption is to ignore compositional effects, and have no internal heating. Then in the non-convecting state, the superadiabatic temperature in the core is

$$T(r) = \Delta T(r_{CMB}^2/r^2 - 1) * r_{ICB}^2/(r_{CMB}^2 - r_{ICB}^2)$$

and there is a flux coming through the ICB driving convection. Differential heating.

Secular cooling is equivalent to a uniform heating, but actually more heat is carried by conduction down adiabatic gradient as r increases, so uniform cooling is a better model.

Model equations 7/36

Compositional convection and boundary conditions

In the geodynamo, compositional convection is at least as important as thermal convection. Modelled as an imposed flux of composition at the the ICB, no flux at the CMB. Requires uniform sink term (equivalent to a secular increase in composition throughout the core).

Stress-free or No-slip? Does make a difference! Since E is far too big, better to have stress-free?

Thermal boundary conditions? On ICB should be

$$\frac{\partial \theta}{\partial r} = L \frac{\partial \theta}{\partial t}$$

$$\frac{\partial \xi}{\partial r} = L \frac{\partial \theta}{\partial t}$$

on the ICB, where θ is temperature difference $T-T_{ref}$ and ξ is difference between composition and its reference state value.

Boundary conditions 8/36

L is a dimensionless parameter dependent on the latent heat of freezing which with conventional values is about 3 (somewhat remarkably!). Physically, cooler fluid in descending plumes freezes iron on the core, releasing a latent heat comparable to that of the secular cooling of the core.

In practice, T=1 on the ICB, T=0 on the CMB is the usual choice.

On CMB, in homogeneous models,

$$\frac{\partial \theta}{\partial r} = 0, \quad \frac{\partial \xi}{\partial r} = 0$$

though there are strong reasons for believing the heat flux is inhomogeneous.

Magnetic boundary conditions: At CMB, match field onto the potential field outside the core.

At the ICB, either assume the inner core is an insulator (simple, but incorrect), or solve the magnetic diffusion equation in the inner core, and match the field across the inner core.

Boundary conditions 9/36

Homogeneous/Heterogeneous CMB boundaries?

Homogeneous boundaries have conditions independent of θ and ϕ .

Heterogeneous boundary conditions take into account that the heat flux carried by mantle convection may vary strongly with latitude and (particularly) longitude. Cold descending plates will give a large heat flux where they hit the CMB.

It is usually the thermal boundary conditions that are taken as heterogeneous.

Seismic observations suggest a plausible form of heterogeneity.

Boundary conditions 10/36

With homogeneous boundary conditions, there is always a solution with no motion (and no field). This becomes unstable as the Rayleigh number is increased through a critical value.

With heterogeneous boundaries, this is no longer true: there is fluid motion at any Ra. At low Ra the form of the convection is determined by boundary flux; at higher Ra this form becomes unstable and the pattern becomes more complex.

When the dynamo comes in, will the magnetic field be locked to the CMB heat flux pattern? This could account for some long term features in the geomagnetic field.

Boundary conditions 11/36

Interpreting dynamo simulations

Dynamo simulations cannot currently be run with Earth-like parameters, and almost certainly never will be. How do we compare outputs with observations?

Viscosity and thermal diffusivity are very small in the core, but much larger in simulations. We have to hope that the small-scale turbulence, which we can't resolve, is enhancing the effective diffusion without doing anything else significant.

How can we test this? Only by exploring the range we can simulate carefully, to see the asymptotic behaviour as viscous and thermal diffusion goes to zero. Also look at simpler plane layer models.

About dynamo simulations 12/36

Rotation rate problem

Additional problem with rotation rate: if we enhance the thermal and viscous diffusion by a factor 10^5 , we have $Pr \sim Pm \sim 1$, but we still have E smaller than we can handle. Effectively, dynamo simulations are run with much slower rotation than the real thing.

With $\nu \approx \eta \approx 2 {\rm m}^2 {\rm s}^{-1}$, $E \sim 3 \times 10^{-9}$, whereas the smallest E we can currently achieve is $E \sim 3 \times 10^{-6}$. This creates a problem, because it means the Rossby number $Ro = U_*/d\Omega$ is much larger in simulations than in the Earth's core.

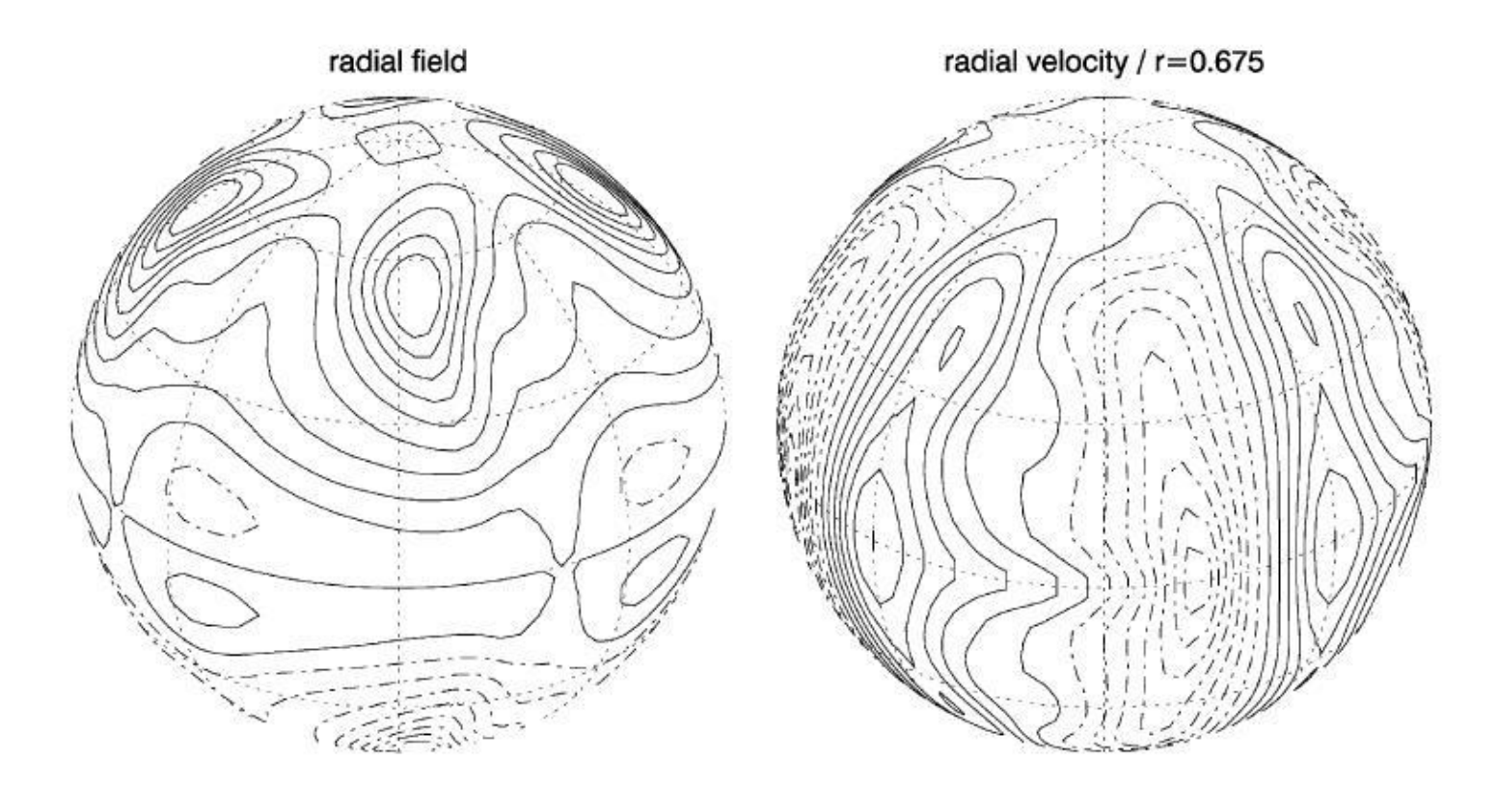
Inertia is more important in simulations than it should be.

Alternative is to increase ν to 10^6 or more, leaving $\kappa \sim \eta$. Then $Pr \sim Pm \sim 10$, and Ω is increased, reducing the Rossby number, and hence the importance of inertia. Evidence that at $\nu = 10^6$ an asymptotic inertia-free regime is reached.

About dynamo simulations 13/36

Benchmark Dynamo

 $E=10^{-3}$, Pr=1, Pm=5, Ra=100. No internal heating, No-slip boundaries. Dynamo steady in (westward) drifting frame. Once started in the m=4 configuration, only harmonics m that are multiples of 4 are present.



About dynamo simulations 14/36

Westward drift in Benchmark Dynamo

The westward drift has angular velocity $\omega \approx 3 \nu/d^2$.

How to estimate ν ? $Pm=\nu/\eta=5$, $\eta=2\,\mathrm{m}^2\,\mathrm{s}^{-1}$ gives $\omega=10^{-11}$. Real thing is $5\times 10^{-4}/2.26\times 10^6\sim 1.4\times 10^{-10}$. Not unreasonable as Ra quite low.

However, $\nu/\Omega d^2=10^{-3}$, $\Omega\sim 7\times 10^{-5}$ gives $\nu=3.6\times 10^5$, giving absurdly large westward drift.

Need scaling laws telling us how models behave in the low E and low Pm limit to make sense of them.

About dynamo simulations 15/36

Spectral methods

Basic idea is to expand the fields in spherical harmonics, and to evolve the coefficients with time. Advantage is that when solution is properly resolved the coefficients of the high order harmonics become exponentially small.

$$\hat{Y}_l^m(\theta,\phi) = P_l^{|m|}(\cos\theta) e^{im\phi}$$

Schmidt normalised Legendre functions are used in geomagnetism, and coefficients are complex.

$$\int_0^{2\pi} \int_0^{\pi} \hat{Y}_l^m \hat{Y}_k^n \sin\theta \, d\theta \, d\phi = 0, \quad m \neq -n, \quad l \neq k$$

$$= 2\pi \int_0^{\pi} \left[P_l^{|m|} (\cos\theta) \right]^2 \sin\theta \, d\theta$$

$$= 2\pi \frac{2(2 - \delta_{m0})}{2l + 1}$$

Spectral methods 16/36

Toroidal-Poloidal expansions

Any velocity and field satisfying $abla \cdot \mathbf{u} =
abla \cdot \mathbf{B} = 0$ can be written

$$\mathbf{u} = \nabla \times (T_u \mathbf{r}) + \nabla \times \nabla \times (P_u \mathbf{r})$$

$$\mathbf{B} = \nabla \times (T_B \mathbf{r}) + \nabla \times \nabla \times (P_B \mathbf{r})$$

automatically reducing from 3 dependent to 2 independent variables.

$$E(\frac{1}{Pm}\frac{\partial}{\partial t} - \nabla^2)\mathbf{u} = \mathbf{N_u} - \nabla\hat{p},$$
$$(\frac{\partial}{\partial t} - \nabla^2)\mathbf{B} = \mathbf{N_B},$$
$$(\frac{\partial}{\partial t} - \frac{Pm}{Pr}\nabla^2)C = N_C,$$

where the nonlinear terms, buoyancy and Coriolis force appear in ${f N}$.

Spectral methods 17/36

Spectral equations

Take $\hat{\mathbf{r}} \cdot \nabla \times$ and $\hat{\mathbf{r}} \cdot$ of the induction equation and $\hat{\mathbf{r}} \cdot \nabla \times$ and $\hat{\mathbf{r}} \cdot \nabla \times \nabla \times$ of the equation of motion to obtain

$$\left(\frac{\partial}{\partial t} - \nabla^2\right) \mathcal{T}_B = \frac{r}{l(l+1)} \hat{\mathbf{r}} \cdot \nabla \times \mathbf{N_B},
 \left(\frac{\partial}{\partial t} - \nabla^2\right) \mathcal{P}_B = \frac{r}{l(l+1)} \hat{\mathbf{r}} \cdot \mathbf{N_B}.$$

and

$$E(\frac{1}{Pm}\frac{\partial}{\partial t} - \nabla^2)\mathcal{T}_u = \frac{r}{l(l+1)}\hat{\mathbf{r}} \cdot \nabla \times \mathbf{N_u},$$

$$E(\frac{1}{Pm}\frac{\partial}{\partial t} - \nabla^2)\mathcal{P}_u = g,$$

$$-\nabla^2 g = \frac{r}{l(l+1)}\hat{\mathbf{r}} \cdot \nabla \times \nabla \times \mathbf{N_u}.$$

The poloidal equation for velocity splits into 2 second order parts.

Spectral methods 18/36

Spectral expansions

Toroidal and poloidal coefficients all expanded in the form

$$A(r,\theta,\phi,t) = \sum_{l=0}^{\infty} \sum_{|m| \le l} A_{lm} \hat{Y}_l^m(\theta,\phi) \tag{*}$$

A real implies $A_{lm}=A_{l,-m}^{st}$ (coefficients are conjugate-symmetric). A_{lm} are functions of r and t only. Now

$$\left(\frac{\partial}{\partial t} - \nabla^2\right)A = \sum_{l=0}^{\infty} \sum_{|m| < l} \left(\frac{\partial}{\partial t} - \frac{1}{r^2} \frac{\partial}{\partial r} r^2 \frac{\partial}{\partial r} + \frac{l(l+1)}{r^2}\right) A_{lm}$$

so our operator now only involves r and t.

At each timestep, we must get the nonlinear right-hand-side in the form (*) and time-step the coefficients of each harmonic separately.

Spectral methods 19/36

Radial dependence and boundary conditions

Either finite differences or Chebyshev polynomials.

$$A_{lm}(r,t) = \sum_{i=0}^{N} a_n(t)T_n(x), \qquad x = -1 + 2(r - r_i)/(r_o - r_i)$$

Chebyshev methods are generally more accurate, but finite difference methods are local, and therefore easier to parallelise. Typically put all variables at one mesh point on one processor.

Insulating boundaries for the induction equation,

$$\mathcal{T}_B = 0, \quad \left(\frac{\partial}{\partial r} - \frac{l}{r}\right) \mathcal{P}_B = 0 \quad \text{on } r_i,$$

$$\mathcal{T}_B = 0, \quad \left(\frac{\partial}{\partial r} + \frac{l+1}{r}\right) \mathcal{P}_B = 0 \quad \text{on } r_o.$$

The potential field of degree l has r-dependence r^l in the inner core and r^{-l-1} in the mantle, and the boundary conditions come from matching the value and radial derivative.

Spectral methods 20/36

Radial formulation for equation of motion

No-slip

$$T = 0, \quad P = 0, \quad \frac{\partial}{\partial r} P_u = 0.$$

Stress-free

$$\left(\frac{\partial}{\partial r} - \frac{1}{r}\right) T_u = 0, \quad P = 0, \quad \frac{\partial^2}{\partial r^2} P_u = 0.$$

A slight complication is that there are 4 bc's on P_u and none on g. Use a Green's function method. For the no-slip case, solve

$$E(\frac{1}{Pm}\frac{\partial}{\partial t} - \nabla^2)\hat{\mathcal{P}}_u = \hat{g}, \quad -\nabla^2\hat{g} = \frac{r}{l(l+1)}\hat{\mathbf{r}} \cdot \nabla \times \nabla \times \mathbf{N_u}$$

with $\partial_r \hat{P}_u = 0$ and $\hat{g} = 0$ on both boundaries. \hat{P}_u won't be zero at the boundaries, but

Spectral methods 21/36

we can add on multiples of P_1 and P_2

$$-E\nabla^2 P_i = g_i, \quad -\nabla^2 g_i = 0, \quad i = 1, 2$$

satisfying $\partial_r \hat{P}_i = 0$, $g_1 = 0,1$, $g_2 = 1,0$ on boundaries r_i,r_o . Required solution is $P_u = \hat{P}_u + aP_1 + bP_2$, a and b being solutions of

$$\begin{bmatrix} P_1(r_i) & P_2(r_i) \\ P_1(r_o) & P_2(r_o) \end{bmatrix} \begin{bmatrix} a \\ b \end{bmatrix} = - \begin{bmatrix} \hat{P}_u(r_i) \\ \hat{P}_u(r_o) \end{bmatrix}$$

 P_1 and P_2 are time-independent, so they can be computed at the start and stored, so the computational cost is negligible, and the method seems robust and accurate.

Spectral methods 22/36

Implicit/Explicit timestepping

The diffusive parts of the spectral equations are time-stepped using implicit Crank-Nicolson, $(y_{t+1}-y_t)/\delta t = 0.5(\nabla^2 y_{t+1} + \nabla^2 y_t) + \text{nonlinear.}$ which allows a larger time-step than an explicit method, and is easy to implement using banded matrices. Unfortunately, we cannot treat the nonlinear terms implicitly.

Usually use Adams-Bashforth, nonlinear = $1.5N_t - 0.5N_{t-1}$.

How do we choose the time-step? Use predictor-corrector method. First find y_{t+1} as normal, then do a corrector by evaluating the nonlinear terms at t+1 and solving again using the Crank-Nicolson formula for the nonlinear terms. Compare predictor and corrector: if very close, increase time-step, if too far apart, reduce time-step.

Spectral methods 23/36

Workload of spectral methods

Most of the computer time is spent evaluating the nonlinear terms.

All differentiating is done in the spectral space, i.e. differentiating Legendre functions, which have standard formulae.

To multiply nonlinear terms, we must evaluate u_r , u_θ etc on a grid, multiply the relevant terms on each grid point, and then convert the values on the grid back to spectral space.

In the ϕ direction fast Fourier transforms can be used to convert between physical and spectral space. Unfortunately, no useful fast Legendre transforms are available. Conversion in θ direction needs N_{θ}^2 operations.

Periodic box is significantly faster than spherical geometry.

Spectral methods 24/36

Finite volume, finite difference methods

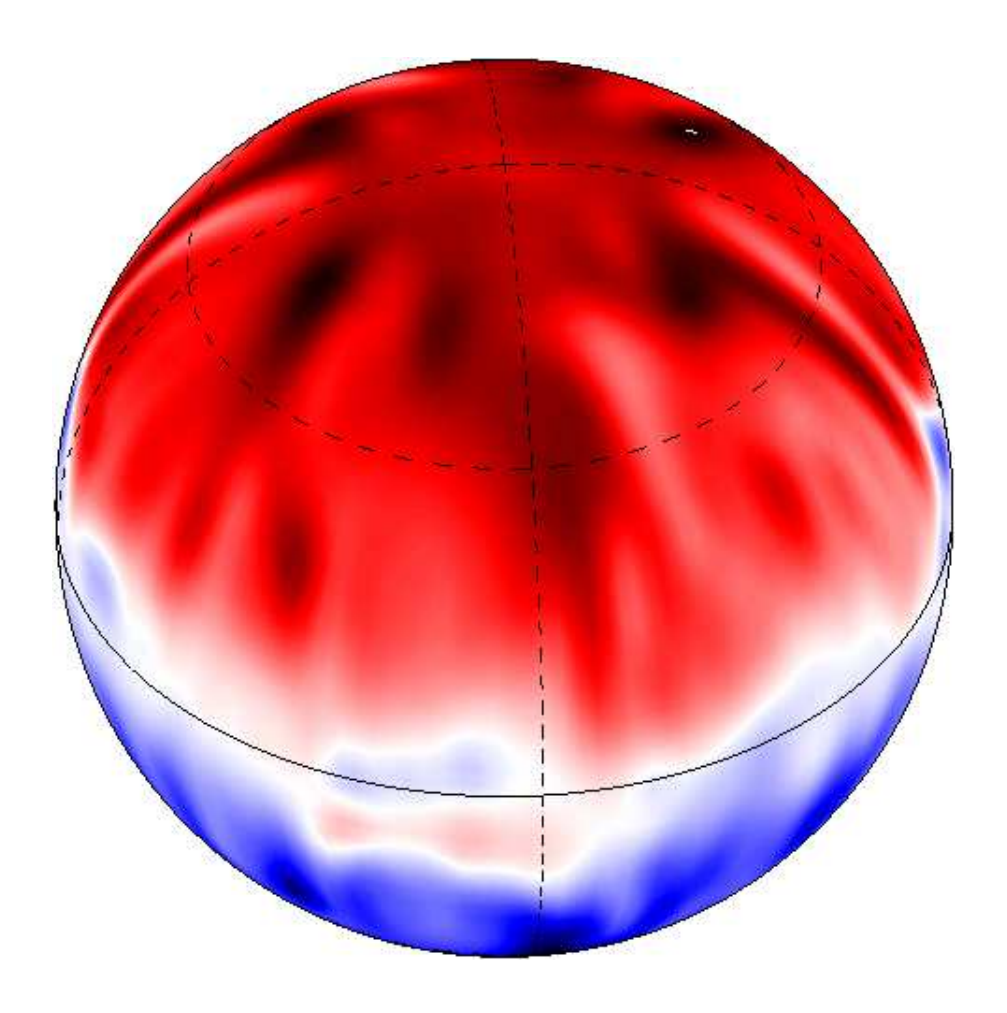
Advantages: local, so better parallelisation. Possibility of fully implicit methods.

Disadvantages: need to avoid high derivatives, so poloidal/toroidal decomposition unattractive. Need to impose solenoidal conditions. Boundary conditions awkward to implement. Less accurate. Pole singularity can only be avoided by using complicated grids.

With today's computers spectral methods seem to have the advantage, but if we can access over 10^3 processors for every day runs, this could change.

Spectral methods 25/36

Results from spectral codes



 $Pr=Pm=1, Ra=750, E=10^{-4}.$ Radial magnetic field snapshot at the CMB

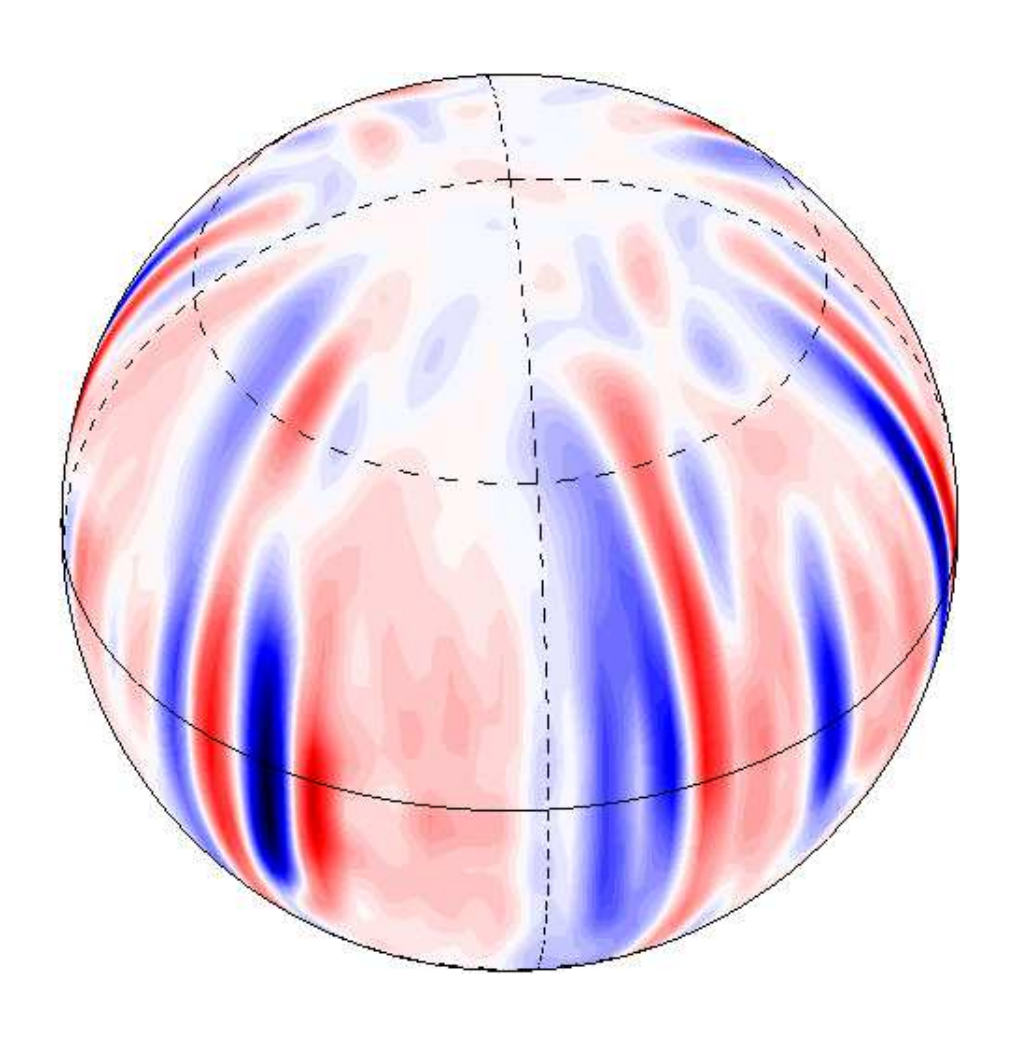
No internal heating. No-slip, fixed temperature, insulating boundaries.

Very dipolar, doesn't reverse. Field slightly weaker at the poles.

Intense flux patches at high latitudes.

Spectral method results 26/36

Velocity field



$$Pr = Pm = 1, Ra = 750, E = 10^{-4}.$$

Radial velocity snapshot at

$$r = 0.8r_{CMB}$$
.

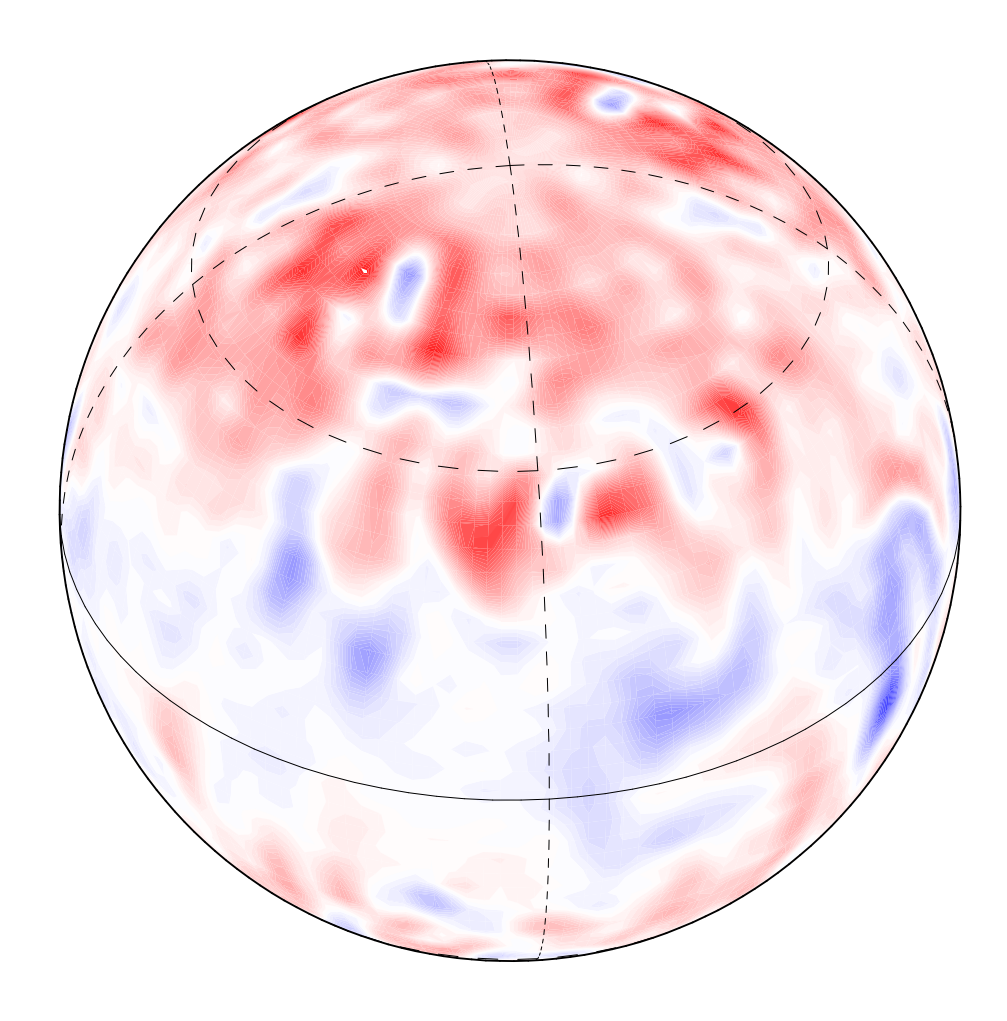
Note the columnar nature of the convection rolls.

Intense flux patches at the top of these columnar rolls.

Pattern propagates westward.

Spectral method results 27/36

Lower Prandtl numbers



$$Pr = Pm = 0.2, Ra = 750,$$

 $E = 10^{-4}.$

Radial magnetic field snapshot at the CMB

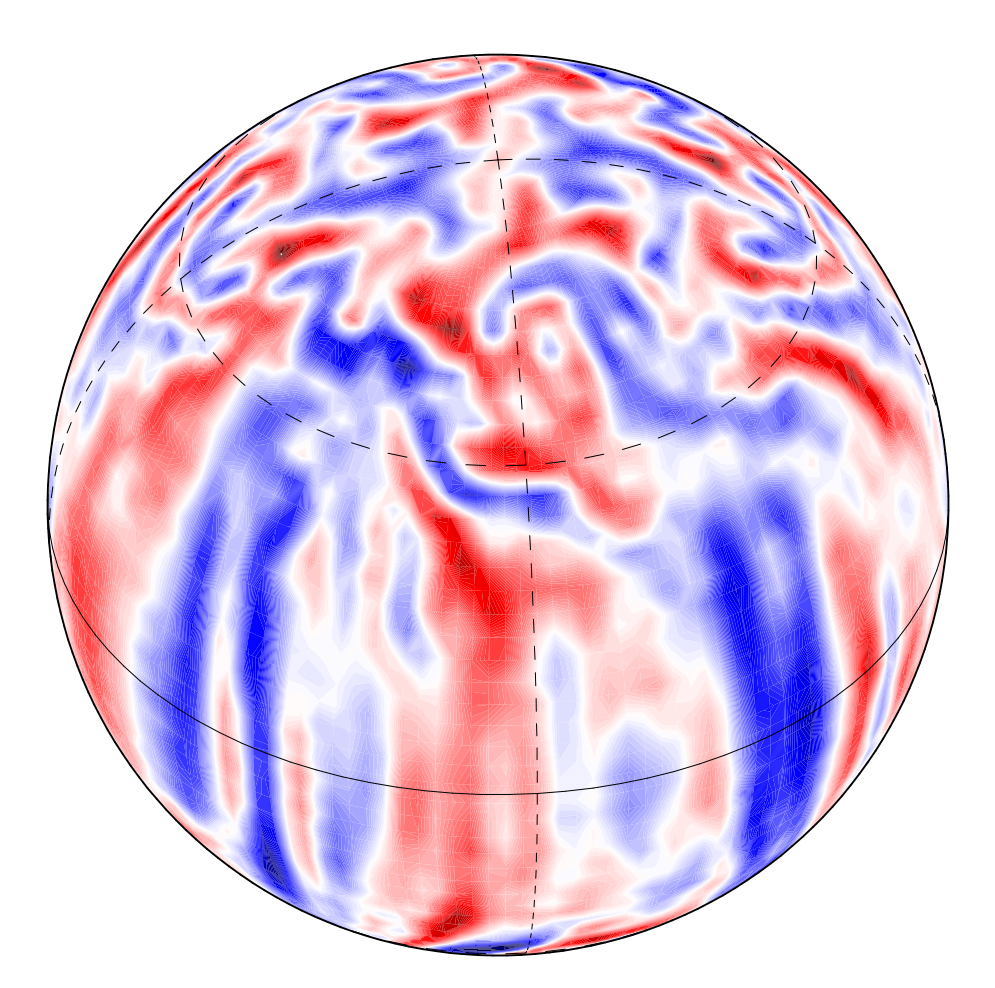
Much less dipolar. Field strength is weaker.

This type of dynamo can reverse.

Rossby number is larger, and inertia is playing a significant role.

Spectral method results 28/36

Flow at lower Prandtl numbers



$$Pr = Pm = 0.2, Ra = 750,$$

 $E = 10^{-4}.$

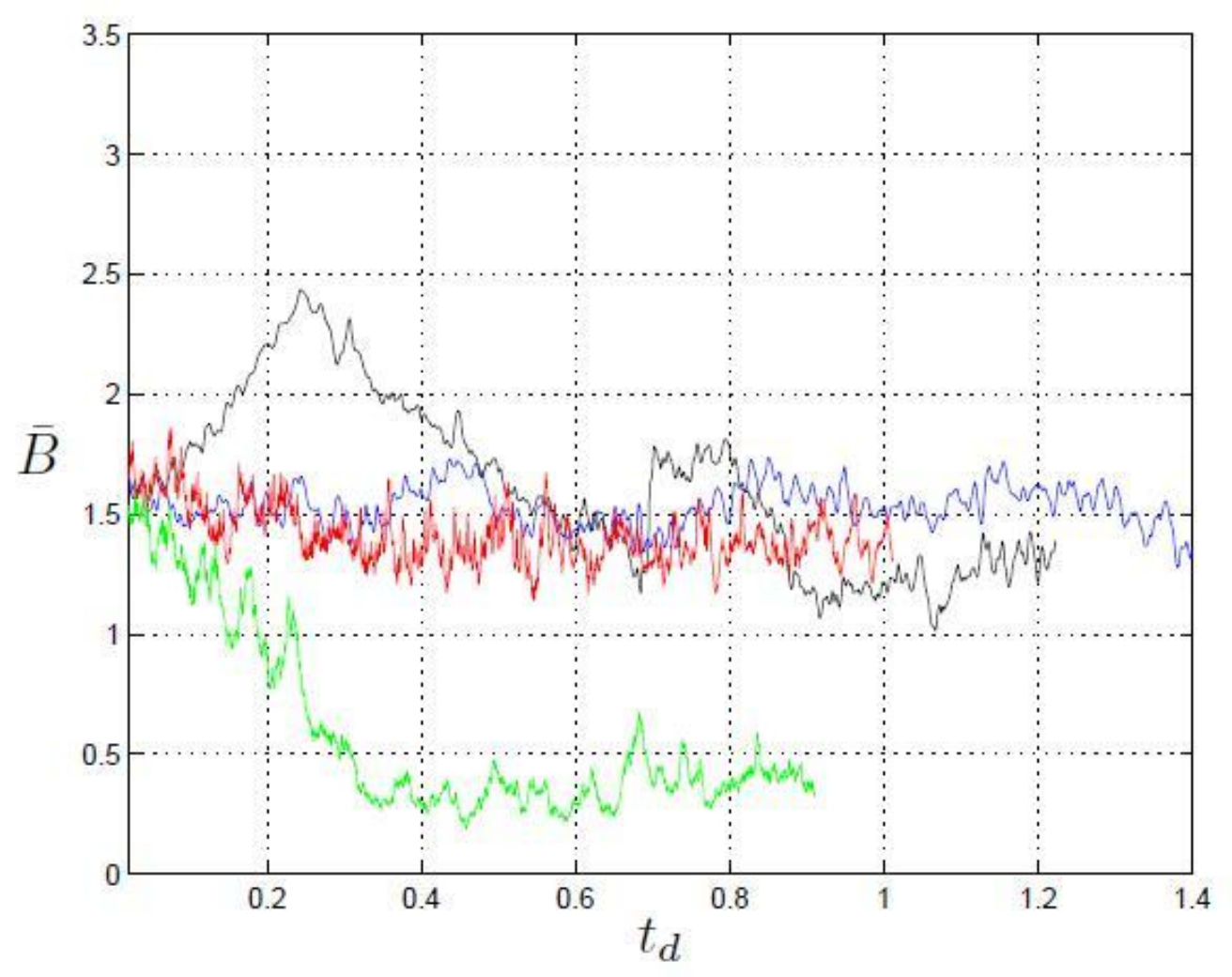
Radial velocity snapshot at $r = 0.8r_{CMB}$.

More activity near the poles, less columnar convection rolls.

Between these patterns lies an Earth-like regime. Unfortunately, at the very low E in the core, we are firmly in the dipolar regime, with inertia very small.

Spectral method results 29/36

Low inertia limit: field

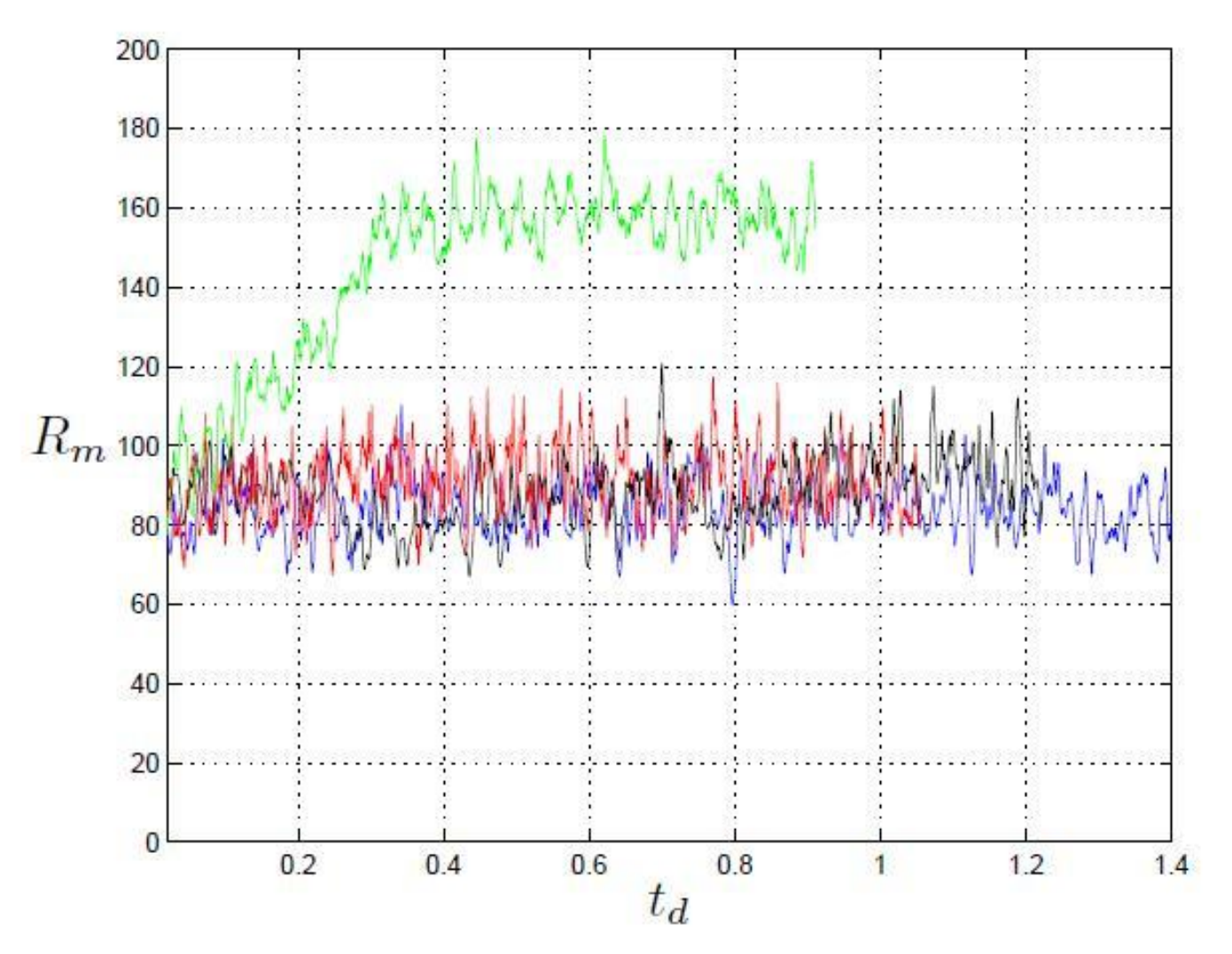


Black:- Pr=Pm=5, Blue:- Pr=Pm=1, Red:- Pr=Pm=0.5, Green:- Pr=Pm=0.2

Sequence of runs showing the low Rossby number inertia-free limit.

Spectral method results 30/36

Low inertia limit: velocity



Black:- Pr=Pm=5, Blue:- Pr=Pm=1,

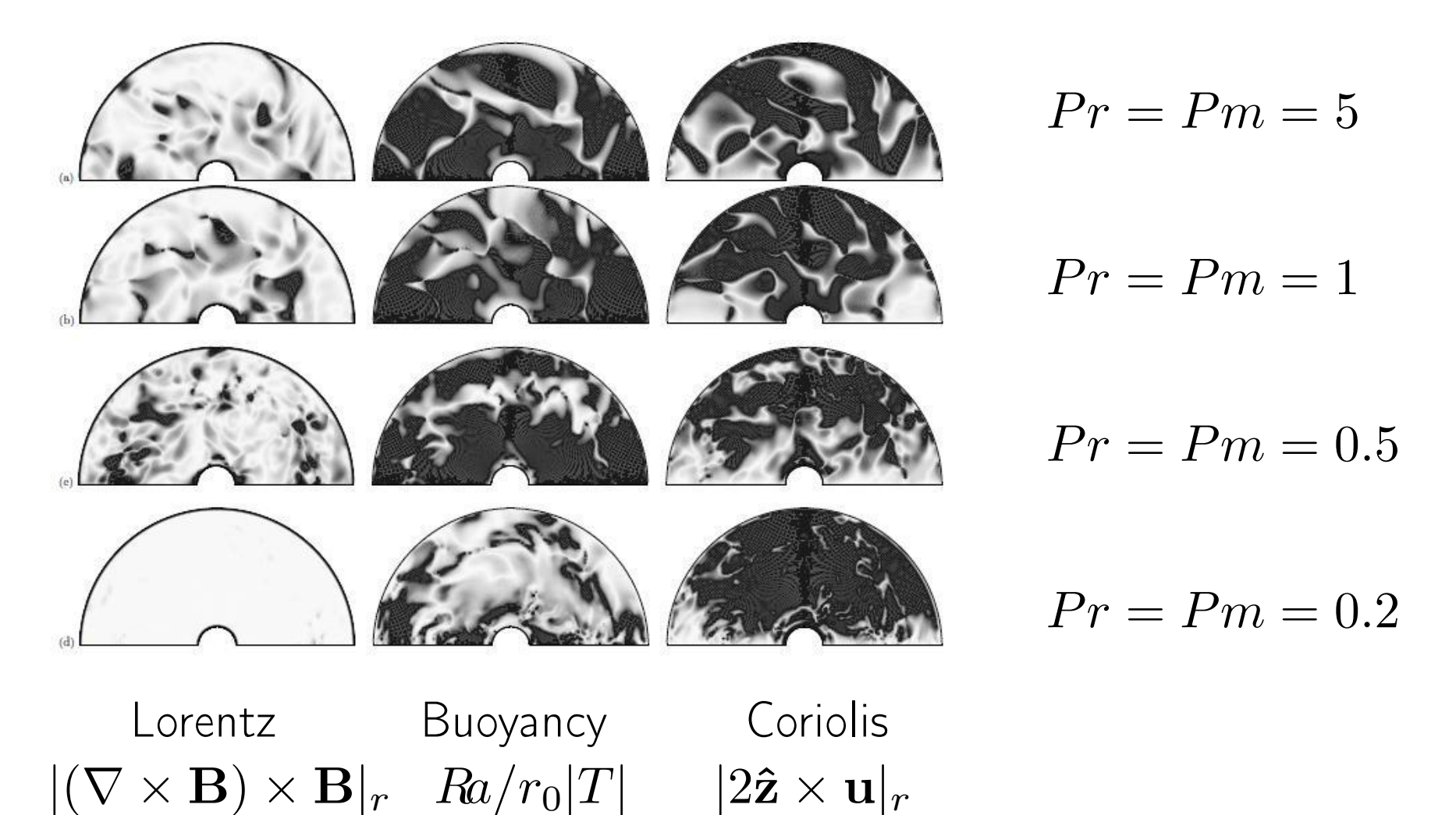
Red:- Pr=Pm=0.5, Green:- Pr=Pm=0.2

Sequence of runs showing the low Rossby number inertia-free limit.

Spectral method results 31/36

Force balance: Lorentz, Buoyancy, Coriolis

Horizontal slice at z=0.5

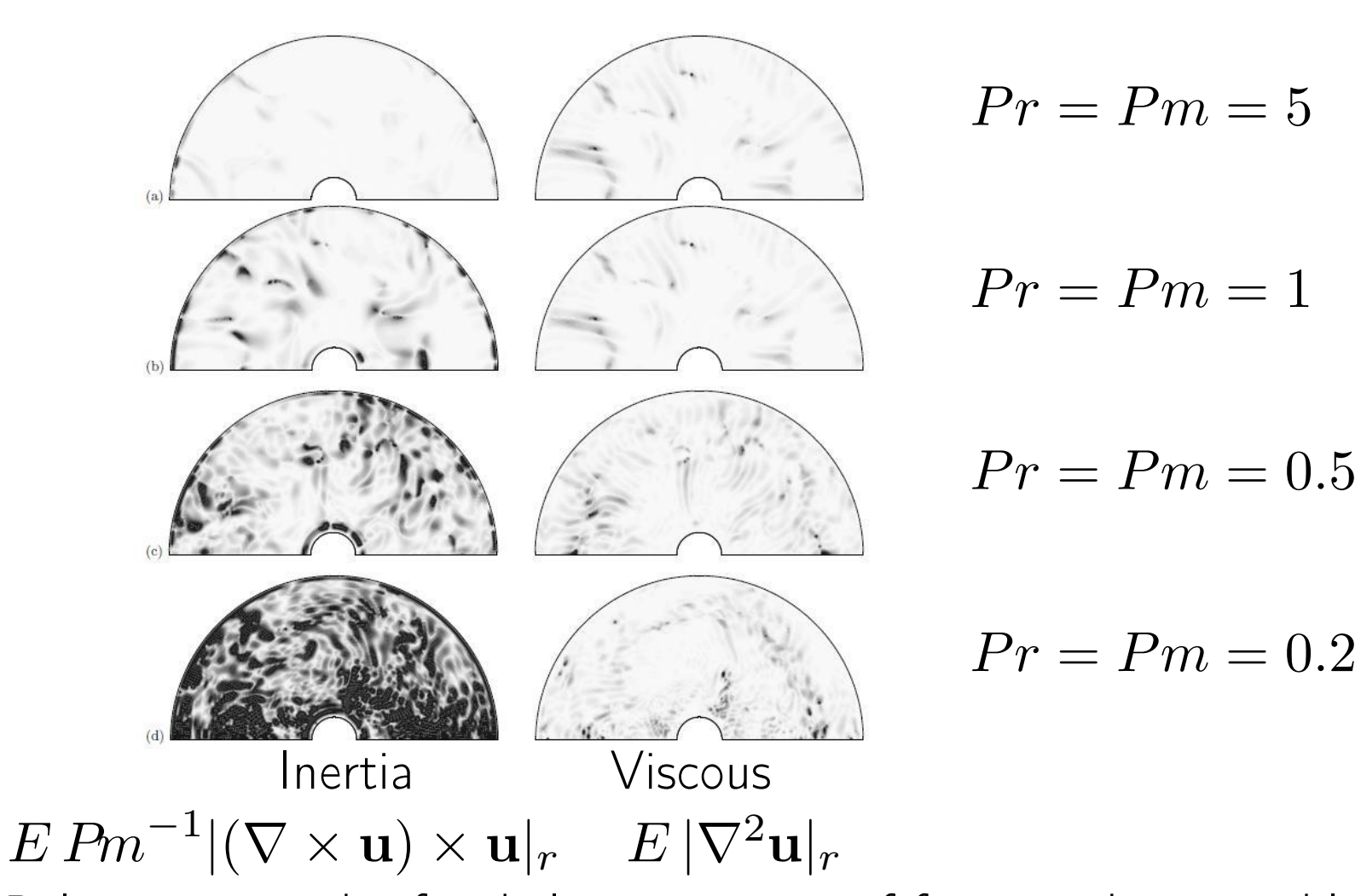


Relative strength of radial components of forces: white =0, black=1.

Spectral method results 32/36

Force balance: Inertia, Viscous

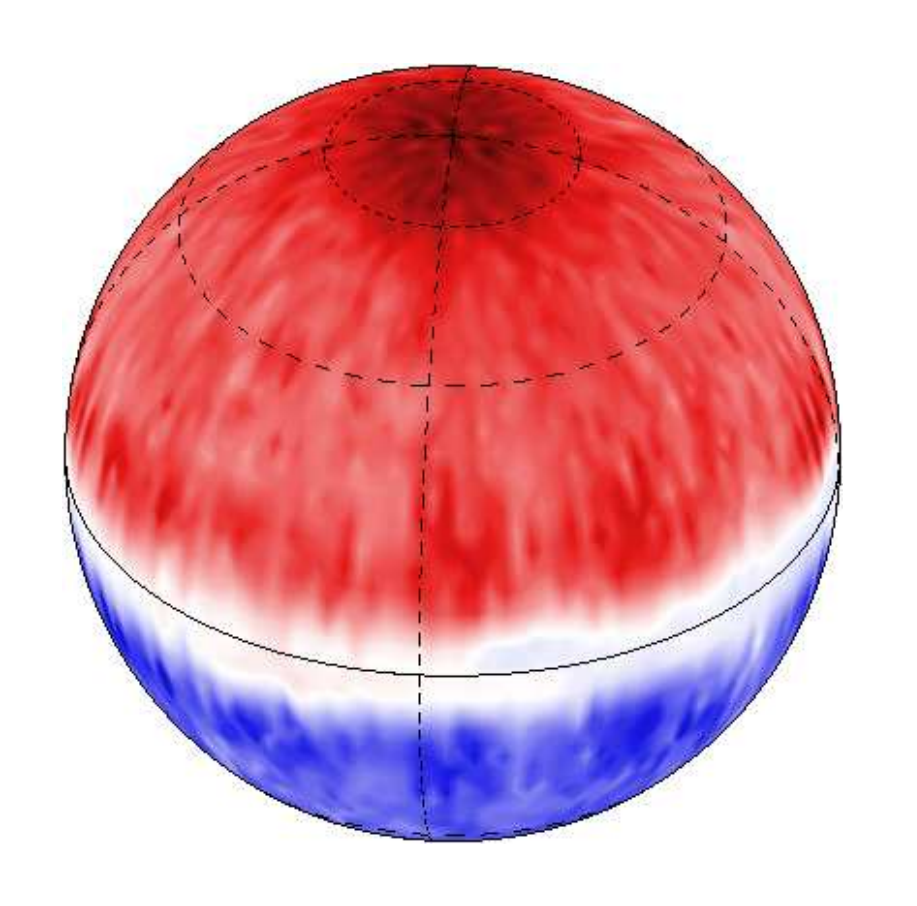
Horizontal slice at z=0.5



Relative strength of radial components of forces: white =0, black=1.

Spectral method results 33/36

Small E, low Pm dynamo



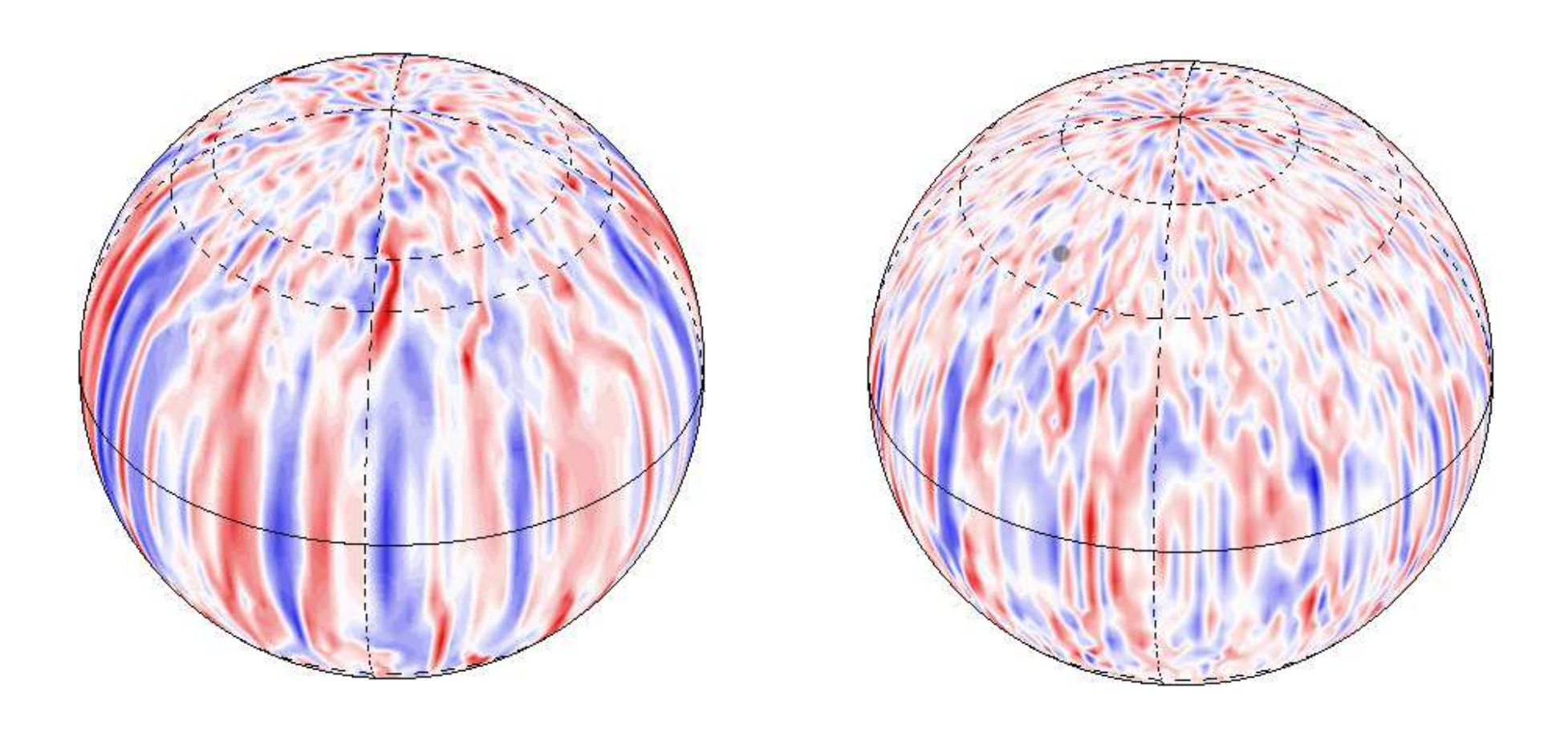
Dipolar dynamo at

$$E=3\times 10^{-6}$$
, $Pr=1$, $Pm=0.1$, $Ra\approx 50Ra_{crit}$.

The magnetic Reynolds number again $Rm\approx 125$, but now fluid Reynolds number much higher $Re\approx 1250$. Field has similar structure to the $E=10^{-4}$ run, but field strength is a little weaker, $\Lambda=B^2/\rho\mu\Omega\eta\approx 0.5$.

Spectral method results 34/36

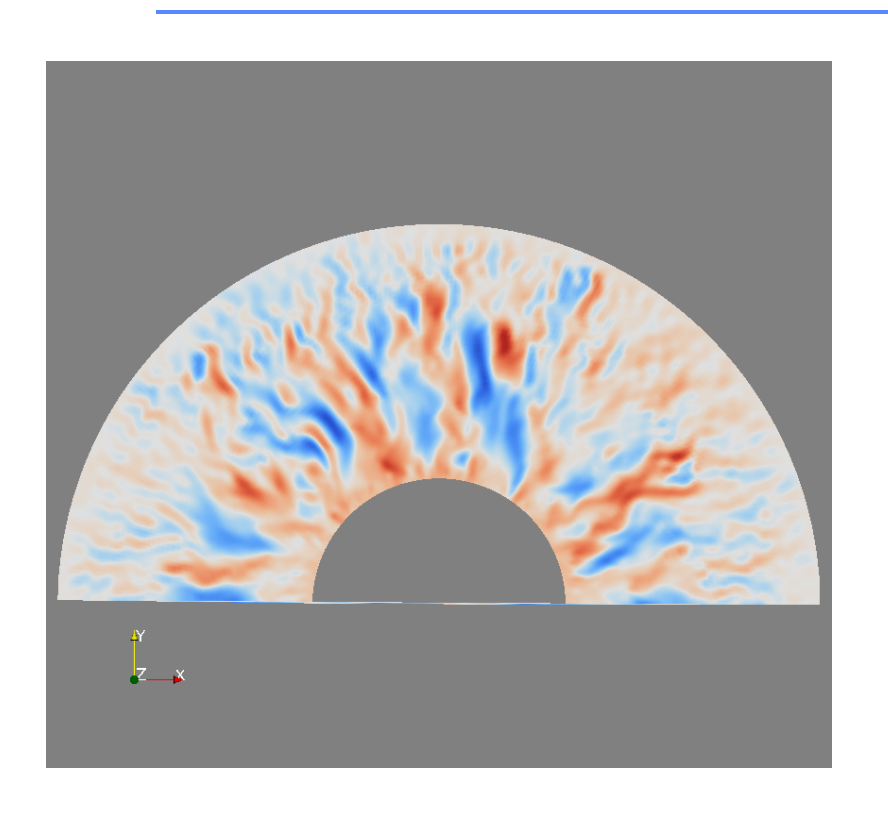
Small E, low Pm dynamo, Flow pattern

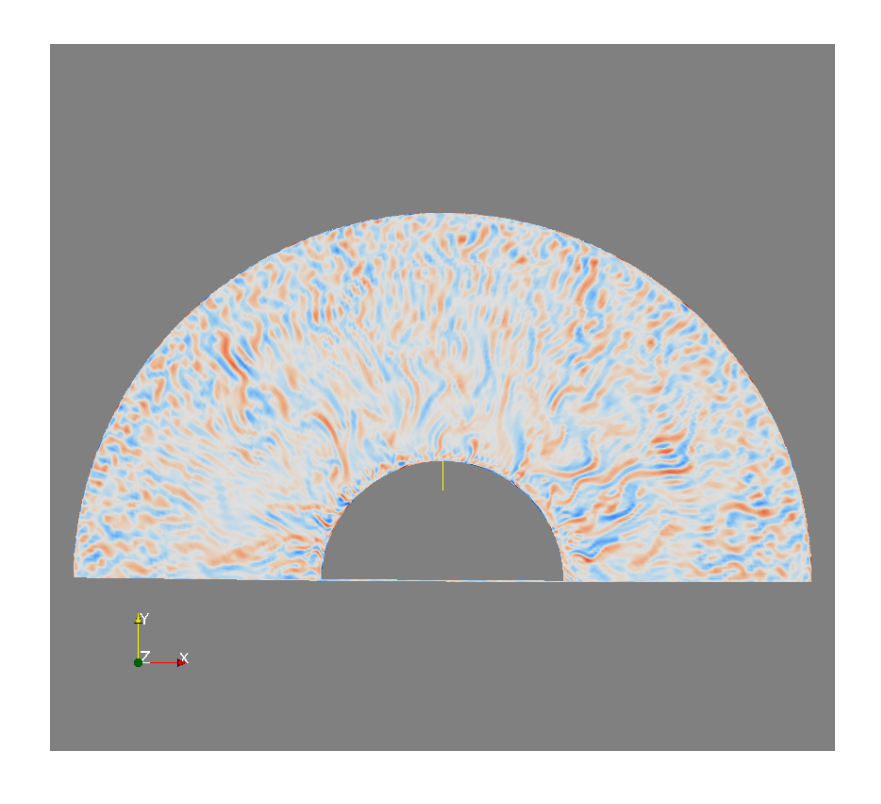


Left: radial velocity at $r=0.5r_0$. Right: radial velocity at $r=0.8r_0$. At lower E the convective columns are much thinner, particularly further out from the ICB.

Spectral method results 35/36

Small E, low Pm dynamo, Scale separation





Left: radial magnetic field at z=0.2. Right: vorticity at z=0.2. Notice that the magnetic field is on a much larger scale in these low Pm calculations. Temperature fluctuations on same scale as magnetic field.

Spectral method results 36/36